Monthly Notices
of the
ROYAL ASTRONOMICAL SOCIETY

MNRAS **473,** 2415–2427 (2018)
Advance Access publication 2017 September 28

doi:10.1093/mnras/stx2505

Properties of magnetically supported dissipative accretion flow around black holes with cooling effects

Biplob Sarkar,[1]★ Santabrata Das[1]★ and Samir Mandal[2]★

[1]*Indian Institute of Technology Guwahati (IITG), Guwahati 781039, Assam, India*
[2]*Indian Institute of Space Science and Technology (IIST), Trivandrum 695547, India*

Accepted 2017 September 24. Received 2017 September 8; in original form 2017 May 22

ABSTRACT

We investigate the global structure of the advection dominated accretion flow around a Schwarzschild black hole where the accretion disc is threaded by toroidal magnetic fields. We consider synchrotron radiative process as an effective cooling mechanism active in the flow. With this, we obtain the global transonic accretion solutions by exploring the variety of boundary conditions and dissipation parameters, namely accretion rate ($\dot{m}$) and viscosity (α_B). The fact that depending on the initial parameters, steady state accretion flows can possess centrifugally supported shock waves. These global shock solutions exist even when the level of dissipation is relatively high. We study the properties of shock waves and observe that the dynamics of the post-shock corona (hereafter, PSC) is regulated by the flow parameters. Interestingly, we find that shock solution disappears completely when the dissipation parameters exceed their critical values. We calculate the critical values of viscosity parameter ($\alpha_B^{\rm cri}$) adopting the canonical values of adiabatic indices as $\gamma = 4/3$ (ultrarelativistic) and 1.5 (seminon-relativistic) and find that in the gas pressure dominated domain, $\alpha_B^{\rm cri} \sim 0.4$ for $\gamma = 4/3$ and $\alpha_B^{\rm cri} \sim 0.27$ for $\gamma = 1.5$, respectively. We further show that global shock solutions are relatively more luminous compared to the shock free solutions. Also, we have calculated the synchrotron spectra for shocked solutions. When the shock is considered to be dissipative in nature, it would have an important implication as the available energy at PSC can be utilized to power the outflowing matter escaped from PSC. Towards this, we calculate the maximum shock luminosity and discuss the observational implication of our present formalism.

Key words: accretion, accretion discs – black hole physics – hydrodynamics – shock waves.

1 INTRODUCTION

The presence of magnetic field is ubiquitous in all astrophysical objects and hence, the accretion discs around black holes are also presumably be magnetized in nature. In the course of accretion process, the magnetic field inside the disc is inherited either from the companion star or from the interstellar medium (Bisnovatyi-Kogan & Ruzmaikin 1974) and these fields are considered as 'frozen' with the accreting matter. In addition, magnetic fields within the disc could originate by the dynamo action as has been proposed by various authors (Torkelsson & Brandenburg 1994; Khanna & Camenzind 1996; Balbus & Hawley 1998). Meanwhile, the importance of magnetic fields in accretion theory was realized by Lynden-Bell (1969); Shakura & Sunyaev (1973), where they reported out that magnetic fields can contribute to the angular momentum transport and explain the unknown nature of disc viscosity. Moreover, Bisnovatyi-Kogan & Blinnikov (1976) pointed out that the presence of magnetic field in the accretion disc seems to be necessary in order to account for the X-ray and gamma-ray emissions from Cyg-X1.

Numerous studies have now conclusively established that magnetic fields indeed play a very important role in the accretion process around black holes. Magnetic fields affect the dynamics of an accretion disc in a number of ways. First, the turbulent magnetic fields generates Maxwell stress which causes efficient angular momentum transport in the disc leading to faster infall of accreting matter into the black hole (Balbus & Hawley 1991). Secondly, observational features such as bipolar outflows and highly collimated jets found in a large number of black hole candidates can be satisfactorily explained due to the presence of a magnetic field. For example, Miller et al. (2006), reported the evidence of magnetic fields helping to drive a highly ionized wind in the stellar mass system GRO J1655-40. Thirdly, heating of the accretion disc may be caused by dissipation of magnetic energy via magnetic reconnection (Hirose, Krolik & Stone 2006; Machida, Nakamura & Matsumoto 2006; Krolik, Hirose & Blaes 2007). Last but not the least, the presence of magnetic fields lead to efficient cooling of the disc because of synchrotron emission by the ionized electrons.

★ E-mail: biplob@iitg.ernet.in (BS); sbdas@iitg.ernet.in (SD); samir@iist.ac.in (SM)

In an accretion disc, differential rotation is the dominant motion over radial infall and this causes the toroidal component of magnetic field to play a major role. We thus consider an accretion disc with turbulent magnetic fields where the azimuthal component of the magnetic field is dominant. The characteristic behaviour of the magnetic and gas pressure are considered to be the same and the total pressure (i.e. gas plus magnetic) provides the vertical support of the disc against gravity. Thus in the standard α-prescription of viscosity, if the total pressure is substituted, there shall be an enhancement of angular momentum transport in the disc since magnetic pressure contributes to the total pressure. Accretion flows with toroidal magnetic fields have been studied both analytically as well as through numerically simulations. Analytical studies on the effect of toroidal magnetic field on the disc have been carried out by Akizuki & Fukue (2006), Begelman & Pringle (2007), Oda et al. (2007), Bu, Yuan & Xie (2009), Oda et al. (2010), Oda et al. (2012), Mosallanezhad, Abbassi & Beiranvand (2014), Samadi, Abbassi & Khajavi (2014), Sarkar & Das (2015), Sarkar & Das (2016). Numerical simulations of accretion disc with toroidal magnetic field around black holes have been carried out by Machida et al. (2006), Hirose et al. (2006), Johansen & Levin (2008). Machida et al. (2006) showed the existence of a magnetically supported, quasi-steady disc during the transition from a low/hard state to a high/soft state in black hole accretion flows. Recent simulation results by Sadowski (2016) also validate the conclusions of Machida et al. (2006).

In order to preserve the inner boundary conditions, flow around a black hole must necessarily be transonic. Accreting matter around a black hole feels a centrifugal force because of its rotation. Matter flowing supersonically near the black hole slows down due to the barrier originating from the centrifugal force. This gives rise to discontinuities in the flow variables in the form of shock waves where the flow undergoes a 'supersonic to subsonic' transition. This phenomenon of shock formation produces centrifugal pressure supported virtual barrier (Chakrabarti 1989) that equivalently refers to the post-shock region (PSC). In absence of the physical boundary layer around the black holes, PSC behaves like an effective boundary layer for the accretion flow for all practical purposes (Chakrabarti 1996; Das et al. 2001b; Chakrabarti & Das 2004; Das 2007; Chattopadhyay & Chakrabarti 2011). The kinetic energy of the flow suffers a sudden reduction due to the shock transition and the thermal energy rises. Hence matter in PSC is heated up and also it gets compressed. Since PSC is hot and compressed compared to the pre-shock matter, it develops an excess thermal gradient force which drives a part of the accreting matter as bidirectional jets/outflows (Chakrabarti 1999; Das et al. 2001b; Chattopadhyay & Das 2007; Singh & Chakrabarti 2011; Kumar & Chattopadhyay 2013; Das et al. 2014a,b; Aktar, Das & Nandi 2015). The soft photons from the outer disc interact with the hot electrons in the PSC and are inverse Comptonized to higher energies producing observable hard photons (Chakrabarti & Titarchuk 1995; Mandal & Chakrabarti 2005; Chakrabarti & Mandal 2006). Also modulation of the PSC causes the phenomena of quasi-periodic oscillations of hard radiations in the X-ray spectrum (Chakrabarti & Manickam 2000).

Recently, Sarkar & Das (2015) have studied magnetized accretion flow around black holes considering the electrons to be cooled by synchrotron emission. For a particular set of injection parameters and different cooling rates, the flow was shown to undergo a shock transition before entering into the black hole. They concluded that apart from viscosity and accretion rate, the plasma β parameter also has a significant effect on the shock dynamics. Sarkar & Das (2016) have studied optically thin magnetized accretion flow around stationary black holes assuming Comptonization of bremsstrahlung radiation to be the active cooling mechanism. They have established that apart from global accretion solutions passing through the inner sonic point studied by Oda et al. (2007, 2012), solutions which pass through the outer sonic point are also possible and such solutions exist over a wide range of outer boundary conditions. In principle, the flow may possess a maximum of three sonic points outside the event horizon (Chakrabarti 1989; Das, Chattopadhyay & Chakrabarti 2001a; Chakrabarti & Das 2004; Sarkar & Das 2013). Depending on the outer boundary conditions, a flow may either pass through the inner sonic point only or may first pass through the outer sonic point and after a shock transition pass through the inner sonic point. Thus, the presence of multiple sonic points is a necessary condition for the formation of shock in the flow. The authors showed that the energy dissipation at the stationary shocks can explain the core radio luminosity of active galactic nuclei. Also, the maximum disc luminosity was estimated to be exceeding 10 per cent of the Eddington luminosity. In global solutions, however, the authors considered the magnetic field strength to be moderate throughout the flow. The bremsstrahlung cooling mechanism employed by Sarkar & Das (2016) is the dominant cooling process in the accretion disc around a supermassive black hole where the magnetic field is expected to be low because of large size of the accretion disc. However, the magnetic field in the accretion disc around a stellar mass black hole is significantly high. Since the disc is arrested by significant magnetic field, the hot electrons in the accretion flow around stellar mass black holes cool primarily by synchrotron emission. When there is significant cooling of the disc, the disc can undergo transition from gas pressure dominated state to magnetic pressure dominated state because of flux conservation at a particular radii (Oda et al. 2007, 2012). The work by Sarkar & Das (2015) is a preliminary investigation of such magnetized discs around stationary black holes employing the synchrotron cooling mechanism. In this work, motivated by these reasons, we make a detailed exploration of the effect of toroidal magnetic fields in magnetically supported accretion discs around black holes assuming synchrotron radiation to be the active cooling mechanism. Thus, to model the dissipative accretion flow, a set of steady state magneto-hydrodynamical equations are considered. The magnetic energy dissipation process governs the heating of the flow. The geometry of space–time around the black hole is described by the Paczyński & Wiita (1980) pseudo-Newtonian potential. With this, we self-consistently calculate the global accretion solution including shock waves and investigate the shock properties in terms of the flow parameters. We establish that a wide range of flow parameters admits shocks in an accretion flow. We identify the critical limits of viscosity parameter, which allows the existence of shocks in the entire regime ranging from magnetic pressure dominated to gas pressure dominated disc. We also quantify the critical limits of accretion rate which allows the existence of shocks in accretion flow and study its variation with plasma β. Furthermore, we present the overall variation of the typical spectra for shocked accretion flows injected with a fixed outer edge conditions having different plasma β values. Finally, considering the dissipative nature of shocks, we present the theoretical estimate of the maximum energy dissipation ($\Delta\mathcal{E}^{\rm max}$) at shock. Using this available energy at shock, we calculate the maximum kinetic power lost from the disc ($L_{\rm shock}^{\rm max}$), which would be useful to understand the core radio luminosities associated with black hole sources.

The outline of the paper is as follows. In Section 2, we present the assumptions and governing equations for our model. In Section 3, we investigate the global accretion solutions with and without shock, shock properties, and the critical limits of viscosity and accretion rate. Next, we present the radiation spectra of the shocked accretion

flows from our model. We also apply our formalism to calculate the maximum energy dissipation at shock and the corresponding shock luminosities. Finally in Section 4, we present the concluding remarks.

2 ACCRETION FLOW MODEL

We account for the magnetic field structure in the accretion disc based on the results of numerical simulations of global magnetohydrodynamic (MHD) accretion flow around black holes in the quasi-steady state (Hirose et al. 2006; Machida et al. 2006). These simulations show that magnetic fields inside the disc are turbulent and dominated by azimuthal component. Hence, based on the findings of these simulations, the magnetic fields are considered as a combination of mean fields and the fluctuating fields. We express the mean fields as $\boldsymbol{B} = (0, < B_\phi >, 0)$, while the fluctuating fields are represented by $\delta\boldsymbol{B} = (\delta B_r, \delta B_\phi, \delta B_z)$. Here, $<>$ signifies the azimuthal average. When the fluctuating components are azimuthally averaged, we assume that they eventually vanish. Accordingly, the azimuthal component of magnetic fields dominates over the radial and vertical components as they are negligible, $| < B_\phi > + \delta B_\phi | \gg |\delta B_r|$ and $|\delta B_z|$. Basically, this renders the azimuthally averaged magnetic field as $< \boldsymbol{B} > = < B_\phi > \hat{\phi}$(Oda et al. 2007).

2.1 Governing equations

In our current model, we consider a thin, axis-symmetric disc around a Schwarzschild black hole of mass $M_{\rm BH}$, in the steady state. We use the Geometric unit system as $2G = M_{\rm BH} = c = 1$, where G is the universal Gravitational constant and c is the speed of light. In this unit system, length, time and velocity are expressed in unit of $r_g = 2GM_{\rm BH}/c^2$, r_g/c and c, respectively. Further, we adopt the cylindrical polar coordinates system (x, ϕ, z) to represent the accretion disc structure where the black hole is located at its origin.

The governing equations that describe the accretion flow around black hole in the steady state are given by

(a) Radial momentum equation:

$$\upsilon\frac{{\rm d}\upsilon}{{\rm d}x} + \frac{1}{\rho}\frac{{\rm d}P}{{\rm d}x} - \frac{\lambda^2(x)}{x^3} + \frac{{\rm d}\Psi}{{\rm d}x} + \frac{\left\langle B_\phi^2\right\rangle}{4\pi x\rho} = 0, \tag{1}$$

where υ is the radial velocity, ρ is the density and λ is the specific angular momentum of the flow, respectively. Here, P denotes the total pressure of the accretion flow which we consider as $P = p_{\rm gas} + p_{\rm mag}$, where $p_{\rm gas}$ is the gas pressure and $p_{\rm mag}$ is the magnetic pressure of the flow, respectively. The gas pressure inside the disc is given by $p_{\rm gas} = R\rho T/\mu$, where R is the gas constant, T is the temperature and μ is the mean molecular weight assumed to be 0.5 for fully ionized hydrogen. The azimuthally averaged magnetic pressure is given by $p_{\rm mag} = < B_\phi^2 > /8\pi$. We define $\beta = p_{\rm gas}/p_{\rm mag}$ and employing this we obtain the total pressure as $P = p_{\rm gas}(\beta + 1)/\beta$. Here, Ψ represents the potential energy. To mimic the general relativistic effects around a stationary black hole, we adopt the pseudo-Newtonian potential (Paczyński & Wiita 1980), which is given by

$$\Psi = -\frac{1}{2(x-1)}. \tag{2}$$

This potential satisfactorily describes the dynamical aspects of general relativity effects in the range $x > 1$ and immensely simplifies the basic equations describing the flow motion in an accretion disc. The last term on the left-hand side represents the magnetic tension force.

(b) Mass Conservation:

$$\dot{M} = 2\pi x\Sigma\upsilon, \tag{3}$$

where $\dot{M}$ represents the mass accretion rate, which is a global constant along the flow. Σ denotes the vertically integrated density of flow (Matsumoto et al. 1984).

(c) Azimuthal momentum equation:

$$\upsilon\frac{{\rm d}\lambda(x)}{{\rm d}x} + \frac{1}{\Sigma x}\frac{\rm d}{{\rm d}x}(x^2 T_{x\phi}) = 0, \tag{4}$$

where the vertically integrated total stress is assumed to be dominated by the $x\phi$ component of the Maxwell stress $T_{x\phi}$. Following the work of Machida et al. (2006), we estimate $T_{x\phi}$ for an advective flow with significant radial velocity (Chakrabarti & Das 2004) as

$$T_{x\phi} = \frac{\langle B_x B_\phi\rangle}{4\pi}h = -\alpha_B(W + \Sigma\upsilon^2), \tag{5}$$

where h denotes the half thickness of the disc. In the right-hand side of equation (5), α_B is the constant of proportionality and W is the vertically integrated pressure (Matsumoto et al. 1984), respectively. In the current model, we take α_B as a global parameter throughout the flow as is considered in Shakura & Sunyaev (1973). When radial advection is negligible, such as for a Keplerian flow, equation (5) simplifies to the original prescription of 'α −model' Shakura & Sunyaev (1973).

Considering the flow to be in hydrostatic equilibrium in the vertical direction, h is expressed as

$$h = \sqrt{\frac{2}{\gamma}}ax^{1/2}(x-1), \tag{6}$$

where a denotes the adiabatic sound speed which is defined as $a = \sqrt{\gamma P/\rho}$, where γ is the adiabatic index. We treat γ as a global parameter and adopt its canonical value as $\gamma = 4/3$ in the subsequent analysis, until otherwise stated.

(d) The entropy generation equation:

$$\Sigma\upsilon T\frac{{\rm d}s}{{\rm d}x} = \frac{h\upsilon}{\gamma-1}\left(\frac{{\rm d}p_{\rm gas}}{{\rm d}x} - \frac{\gamma p_{\rm gas}}{\rho}\frac{{\rm d}\rho}{{\rm d}x}\right) = Q^- - Q^+, \tag{7}$$

where s and T denote the specific entropy and the local temperature of the flow, respectively. Here, Q^+ and Q^- represent the vertically integrated heating and cooling rates. The heating of the flow takes place due to the thermalization of magnetic energy through the magnetic reconnection mechanism (Hirose et al. 2006; Machida et al. 2006) and therefore is given by

$$Q^+ = \frac{< B_x B_\phi >}{4\pi}xh\frac{{\rm d}\Omega}{{\rm d}x} = -\alpha_B(W + \Sigma\upsilon^2)x\frac{{\rm d}\Omega}{{\rm d}x}, \tag{8}$$

where Ω refers to the local angular velocity of the flow.

In an accretion disc, the cooling of the flow is governed by the various radiative processes such as bremsstrahlung, synchrotron or Comptonization of bremsstrahlung and synchrotron photons. In this work, since the accretion flow is magnetized in nature, synchrotron process becomes effective to cool the flow and the cooling rate due to the synchrotron radiation is given by (Shapiro & Teukolsky 1983)

$$Q^- = \frac{Sa^5\rho h}{\upsilon x^{3/2}(x-1)}\frac{\beta^2}{(1+\beta)^3}$$

with

$$S = 1.048\times10^{18}\frac{\dot{m}\mu^2 e^4}{I_n m_{\rm e}^3\gamma^{5/2}}\frac{1}{2GM_\odot c^3}, \tag{9}$$

where e and $m_{\rm e}$ denote the charge and mass of the electron, respectively. And, $k_{\rm B}$ is the Boltzmann constant, μ is the mean

molecular weight, $I_n = (2^n n!)^2/(2n+1)!$ and $n = 1/(\gamma - 1)$. Following Chattopadhyay & Chakrabarti (2002), we estimate the electron temperature as $T_e = \sqrt{m_e/m_p}T_p$, where the coupling between the ions and electrons, if any, is ignored and m_p refers to the mass of the ion. In the subsequent sections, we express accretion rate in units of Eddington rate ($\dot{M}_{edd} = 1.39 \times 10^{17} \times M_{BH}/M_\odot$ g s^{-1}) and we denote it by $\dot{m}$. Furthermore, in account of the energy loss of the flow, we neglect the contribution of the bremsstrahlung emission because it is regarded as a very inefficient cooling process for stellar mass black hole systems (Chattopadhyay & Chakrabarti 2000; Das 2007).

(e) Radial advection of the toroidal magnetic flux:
We describe the advection rate of the toroidal magnetic flux by considering the induction equation and it is expressed as

$$\frac{\partial < B_\phi > \hat{\phi}}{\partial t} = \nabla \times \left(\vec{v} \times < B_\phi > \hat{\phi} - \frac{4\pi}{c}\eta \vec{j} \right), \tag{10}$$

where $\vec{v}$ denotes velocity vector, η is the resistivity and $\vec{j} = c(\nabla \times < B_\phi > \hat{\phi})/4\pi$ refers to the current density. Here, equation (10) is azimuthally averaged. Since the Reynolds number (R_m) is very large in the case of accretion disc, on account of very large length scale, we neglect the magnetic-diffusion term. Moreover, we neglect the dynamo term in this study. In the steady state, the resulting equation is then vertically averaged assuming that the averaged toroidal magnetic fields vanish at the disc surface. With this, we obtain the advection rate of the toroidal magnetic flux as (Oda et al. 2007)

$$\dot{\Phi} = -\sqrt{4\pi} v h B_0(x), \tag{11}$$

where

$$B_0(x) = \langle B_\phi \rangle (x; z = 0) = 2^{5/4}\pi^{1/4}(RT/\mu)^{1/2}\Sigma^{1/2}h^{-1/2}\beta^{-1/2}$$

represents the azimuthally averaged toroidal magnetic field confined in the disc equatorial plane. In equation (11), the magnetic flux advection rate ($\dot{\Phi}$) is expected to vary in the radial direction when both the dynamo term and the magnetic diffusion term is present. Global three-dimensional MHD simulation of Machida et al. (2006) indicates that the magnetic flux advection rate varies as $\dot{\Phi} \propto 1/x$, when the disc is in the quasi-steady state. In the present context, the computation of the magnetic diffusion term and the dynamo terms is beyond the scope the paper and therefore, based on the above findings, we adopt a parametric relation between $\dot{\Phi}$ and x, which is given by (Oda et al. 2007)

$$\dot{\Phi}(x; \zeta, \dot{M}) \equiv \dot{\Phi}_{edge}(\dot{M}) \left(\frac{x}{x_{edge}} \right)^{-\zeta}, \tag{12}$$

where $\dot{\Phi}_{edge}$ is the advection rate of the toroidal magnetic flux at the outer edge of the disc (x_{edge}). When $\zeta = 0$, the conservation of magnetic flux in the radial direction is restored. For $\zeta > 0$, the magnetic flux increases as the accreting matter approaches the black hole horizon. In this analysis, we consider ζ as a global constant and fix its value as $\zeta = 1$ for representation, unless stated otherwise.

2.2 Sonic point analysis

In the process of accretion on to the black hole, infalling matter starts its journey from the outer edge of the disc with negligible radial velocity and subsequently crosses the black hole horizon with the velocity comparable to the speed of light. This findings evidently demand that during accretion, infalling matter must change its sonic character smoothly from subsonic state to supersonic state before falling in to the black hole. The radial coordinate where accreting matter encounter such sonic transition is known as sonic point. In the next paragraphs, we carry out the sonic point analysis of the accretion flow by simultaneously solving equations (1), (3), (4), (7), (11) and (12) which is expressed as

$$\frac{dv}{dx} = \frac{N}{D}, \tag{13}$$

where the numerator N is given by

$$\begin{aligned} N = {} & \frac{Sa^5}{vx^{3/2}(x-1)}\frac{\beta^2}{(1+\beta)^3} + \frac{2\alpha_B^2 I_n (a^2 g + \gamma v^2)^2}{\gamma^2 x v} \\ & + \frac{2\alpha_B^2 g I_n a^2 (5x-3)(a^2 g + \gamma v^2)}{\gamma^2 v x (x-1)} \\ & - \left[\frac{\lambda^2}{x^3} - \frac{1}{2(x-1)^2} \right] \left[\frac{[3+\beta(\gamma+1)]v}{(\gamma-1)(1+\beta)} - \frac{4\alpha_B^2 g I_n (a^2 g + \gamma v^2)}{\gamma v} \right] \\ & - \frac{v a^2 (5x-3)}{x(\gamma-1)(x-1)} \frac{\left(\beta + \frac{3}{2\gamma}\right)}{(1+\beta)} - \frac{4\lambda\alpha_B I_n (a^2 g + \gamma v^2)}{\gamma x^2} \\ & - \frac{8\alpha_B^2 I_n a^2 g (a^2 g + \gamma v^2)}{\gamma^2 v (1+\beta) x} + \frac{2[3+\beta(\gamma+1)]a^2 v}{\gamma(\gamma-1)(1+\beta)^2 x} \\ & - \frac{a^2 v}{\gamma(\gamma-1)(1+\beta)(x-1)} - \frac{a^2 v(4\zeta - 1)}{2\gamma x(\gamma-1)(1+\beta)} \end{aligned} \tag{13a}$$

and the denominator D is given by

$$\begin{aligned} D = {} & \frac{2a^2}{(\gamma-1)} \left[\frac{2}{\gamma(1+\beta)} + \frac{\beta}{1+\beta} \right] - \frac{[3+(\gamma+1)\beta]v^2}{(\gamma-1)(1+\beta)} \\ & + \frac{2\alpha_B^2 I_n (a^2 g + \gamma v^2)}{\gamma} \left[(2g-1) - \frac{a^2 g}{\gamma v^2} \right]. \end{aligned} \tag{13b}$$

Here, we write $g = I_{n+1}/I_n$.

Further, we obtain the gradient of sound speed, angular momentum and plasma β, respectively as

$$\begin{aligned} \frac{da}{dx} = {} & \left(\frac{a}{v} - \frac{\gamma v}{a} \right) \frac{dv}{dx} + \frac{\gamma}{a} \left[\frac{\lambda^2}{x^3} - \frac{1}{2(x-1)^2} \right] \\ & + \frac{(5x-3)a}{2x(x-1)} - \frac{2a}{(1+\beta)x}, \end{aligned} \tag{14}$$

$$\begin{aligned} \frac{d\lambda}{dx} = {} & -\frac{\alpha_B x (a^2 g - \gamma v^2)}{\gamma v^2}\frac{dv}{dx} + \frac{2\alpha_B a x g}{\gamma v}\frac{da}{dx} \\ & + \frac{\alpha_B (a^2 g + \gamma v^2)}{\gamma v}, \end{aligned} \tag{15}$$

$$\begin{aligned} \frac{d\beta}{dx} = {} & \frac{(1+\beta)}{v}\frac{dv}{dx} + \frac{3(1+\beta)}{a}\frac{da}{dx} + \frac{1+\beta}{x-1} \\ & + \frac{(1+\beta)(4\zeta-1)}{2x}. \end{aligned} \tag{16}$$

It is already pointed out that the trajectory of the accretion flow around black hole must be smooth along the streamline and hence, dv/dx must be real and finite always. From equation (13 b), however we infer that the denominator D may vanish at some radial distance between the outer edge of the disc and the horizon. In order to maintain the flow to be smooth everywhere along the streamline, the point where D goes to zero, N must also tend to be zero there. Indeed, the location where both N and D vanish simultaneously

is called as sonic point as the infalling matter becomes transonic there. Following this, we obtain two conditions at the sonic point as $N = 0$ and $D = 0$. Setting D to zero, we have the expression of Mach number ($M = \upsilon/a$) at the sonic point (x_c) as

$$M(x_c) = \sqrt{\frac{-m_2 - \sqrt{m_2^2 - 4m_1m_3}}{2m_1}}, \tag{17}$$

where

$$m_1 = 2\alpha_B^2 I_n \gamma^2(1+\beta_c)(\gamma-1)(2g-1) - \gamma^2(3+(\gamma+1)\beta_c)$$

$$m_2 = 2\gamma(2+\gamma\beta_c) + 4\alpha_B^2 I_n \gamma g(1+\beta_c)(g-1)(\gamma-1)$$

$$m_3 = -2\alpha_B^2 I_n g^2(1+\beta_c)(\gamma-1).$$

Using the remaining sonic point condition $N = 0$, we get an algebraic equation of the sound speed at x_c which is given by

$$\mathcal{A}a^3(x_c) + \mathcal{B}a^2(x_c) + \mathcal{C}a(x_c) + \mathcal{D} = 0, \tag{18}$$

where

$$\mathcal{A} = \frac{S}{x_c^{3/2}(x_c-1)}\frac{\beta_c^2}{(1+\beta_c)^3},$$

$$\mathcal{B} = \frac{2\alpha_B^2 I_n \left(g+\gamma M_c^2\right)^2}{\gamma^2 x_c} + \frac{2\alpha_B^2 I_n g(5x_c-3)\left(g+\gamma M_c^2\right)}{\gamma^2 x_c(x_c-1)} - \frac{M_c^2(5x_c-3)}{x_c(\gamma-1)(x_c-1)}\frac{\left(\beta_c+\frac{3}{2\gamma}\right)}{(1+\beta_c)} - \frac{8\alpha_B^2 I_n g\left(g+\gamma M_c^2\right)}{\gamma^2(1+\beta_c)x_c} + \frac{2[3+\beta_c(\gamma+1)]M_c^2}{\gamma(\gamma-1)(1+\beta_c)^2 x_c} - \frac{M_c^2}{\gamma(\gamma-1)(1+\beta_c)(x_c-1)} - \frac{(4\zeta-1)M_c^2}{2\gamma(\gamma-1)(1+\beta_c)x_c},$$

$$\mathcal{C} = -\frac{4\lambda_c\alpha_B I_n M_c\left(g+\gamma M_c^2\right)}{\gamma x_c^2},$$

$$\mathcal{D} = -\left[\frac{\lambda_c^2}{x_c^3} - \frac{1}{2(x_c-1)^2}\right] \times \left[\frac{[3+\beta_c(\gamma+1)]M_c^2}{(1+\beta_c)(\gamma-1)} - \frac{4\alpha_B^2 g I_n\left(g+\gamma M_c^2\right)}{\gamma}\right].$$

Here, the quantities with subscript 'c' indicate their values measured at the sonic point.

Upon solving equation (18) for a set of input parameters of the flow, we calculate the sound speed at x_c and then find the radial velocity of the flow using equation (17). Using these quantities in equation (13), we investigate the properties of the sonic point. At x_c, $\mathrm{d}\upsilon/\mathrm{d}x$ generally possesses two values; one corresponds to accretion flow and the other for wind solution. When both the values of $\mathrm{d}\upsilon/\mathrm{d}x$ are real and of opposite sign, such a sonic point has special significance as the global transonic solution only passes through it. Sonic point of this kind is called the saddle type sonic point (Chakrabarti & Das 2004). In this work, we are mainly interested to study the properties of the global accretion flow around the black holes and hence, the wind solutions are left aside for future study.

3 RESULTS

We simultaneously solve the differential equations (13), (14), (15) and (16) for a given set of flow parameters to obtain the global transonic accretion solution around black hole. In this analysis, $\dot{m}$, α_B and γ are treated as the global parameters of the flow. And, three additional parameters are required in order to start the numerical integration of the above equations from a reference point ($x_{\rm ref}$). These three parameters are $x_{\rm ref}$, angular momentum at $x_{\rm ref}$ ($\lambda_{\rm ref}$) and plasma β at $x_{\rm ref}$ ($\beta_{\rm ref}$), respectively and they are treated as the local parameters. With this, we obtain the transonic global accretion solutions that may contain shock waves. It is to be noted that we present angular momentum ($\lambda_{\rm ref}$) in terms of Keplerian angular momentum λ_K ($\equiv \sqrt{x_{\rm ref}^3/2(x_{\rm ref}-1)^2}$) all throughout the paper.

3.1 Global accretion solutions

In Fig. 1, we present the 'phase space diagrams' of accretion solutions where the Mach number ($M = \upsilon/a$) is plotted as function of the logarithmic radial distance (x). Here, we consider the inner sonic point ($x_{\rm in}$) as the reference point ($x_{\rm ref}$) and choose $x_{\rm in} = 2.41$. The angular momentum and the plasma β at $x_{\rm in}$ are kept fixed as $\lambda_{\rm in} = 0.9327\lambda_K$ and $\beta_{\rm in} = 20$, respectively. Moreover, we choose $\alpha_B = 0.02$, $\dot{m} = 0.004$ and $\gamma = 4/3$. With this set of parameters, we integrate equations (13–16) starting from the inner sonic point once inward up to black hole horizon and then outward up to a large distance (equivalently 'outer edge of the disc'). Upon joining them, ultimately we get a global transonic accretion solution as it connects the outer edge of the disc with the black hole horizon. In the figure, this solution is plotted with long-dashed curve and marked as 'a'. The arrow indicates the direction of the flow. Next, we decrease plasma β at $x_{\rm in}$ as $\beta_{\rm in} = 7$ and calculate the global transonic accretion solution keeping the remaining flow parameters fixed. The obtained result is plotted using short-dashed curve and marked with

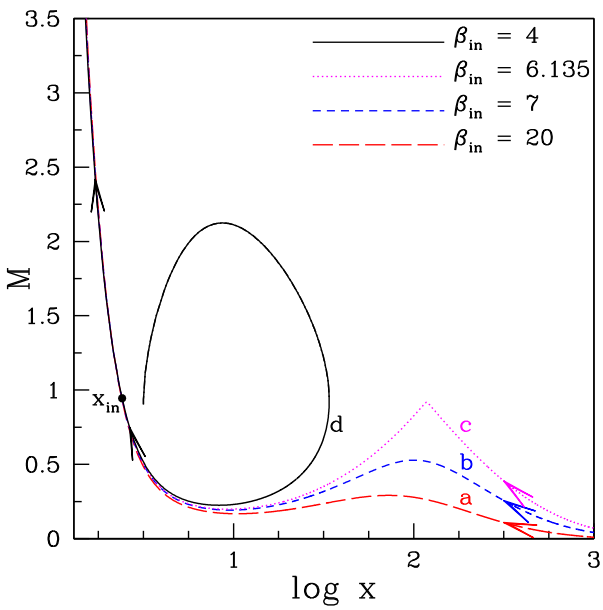

Figure 1. Radial dependence of Mach number ($M = \upsilon/a$) of the accreting matter for different values of plasma β ($\beta_{\rm in}$) at the inner sonic point $x_{\rm in} = 2.41$. Here, $\lambda_{\rm in} = 0.9327\lambda_K$, $\alpha_B = 0.02$ and $\dot{m} = 0.004$. Long-dashed and short-dashed curves represent the results for $\beta_{\rm in} = 20$ and 7, respectively. For the same set of flow parameters, the minimum values of plasma β that provides the accretion solution connecting the inner sonic point to up to a large distance (equivalently 'outer edge of the disc') is obtained as $\beta_{\rm in}^{\rm cri} = 6.135$ and the solution is depicted with the dotted curve. When $\beta_{\rm in} < \beta_{\rm in}^{\rm cri}$, accretion solutions fail to connect to the outer edge of the disc and such a representative solution is depicted by the solid curve for $\beta_{\rm in} = 4$.

'b'. We observe that the qualitative feature of the solution 'b' is very much similar to solution 'a'. With the gradual decrease of $\beta_{\rm in}$, we obtain a critical value $\beta_{\rm in}^{\rm cri} = 6.135$ corresponding to the chosen set of flow parameters, which is the minimum value of $\beta_{\rm in}$ that provides a transonic global accretion solution passing through the inner sonic point. This solution is plotted with the dotted curve and marked as 'c'. Needless to mention that the curves marked with 'a–c' represent the results identical to the well-known advection dominated accretion flow (ADAF) solutions around black holes (Narayan, Kato & Honma 1997; Oda et al. 2007). When $\beta_{\rm in} < \beta_{\rm in}^{\rm cri}$, transonic accretion solution fails to extend up to the outer edge of the disc and does not represent a complete global accretion solution. For representation, we obtain such a solution for $\beta_{\rm in} = 4$, which is illustrated with a solid curve and marked as 'd'.

Apparently, solution 'd' in Fig. 1 does not connect the black hole horizon with the outer edge of the disc. However, solutions of this kind are potentially promising in the sense that they can be joined with another transonic accretion solution passing through the outer sonic point ($x_{\rm out}$) via shock transition. The complete description of such a composite global accretion solution can be visualized in the following manner. The rotating subsonic accretion flow at the outer edge of the disc slowly gains its radial velocity due to the attraction of gravity. Subsequently, flow becomes supersonic after passing through $x_{\rm out}$ and continues to proceed towards the black hole. In the vicinity of the black holes, since the viscous time-scale greatly exceeds over the infall time-scale, the angular momentum transport due to viscosity becomes feeble and therefore, centrifugal repulsion becomes comparable to the gravitational force there. As a result, infalling matter experiences a virtual barrier and eventually slows down. This causes the piling of matter and develops local turbulence that establishes entropy generation leading towards the triggering of shock transition provided the shock conditions are satisfied. In fact, according to the second law of thermodynamics, the presence of the shock wave in accretion flows is thermodynamically preferred when the post-shock flow possesses high entropy content (Becker & Kazanas 2001). The entropy content of a dissipative accretion flow is obtained as (Chakrabarti 1996)

$$\dot{\mathcal{M}}(x) \propto \left(\frac{\beta}{1+\beta}\right)^{n} a^{(2n+1)} \upsilon x^{3/2}(x-1), \tag{19}$$

where $n = 1/(\gamma - 1)$ is the polytropic index of the flow. In the absence of any dissipative processes, namely viscosity and/or radiative cooling, $\dot{\mathcal{M}}$ remains constant throughout the flow except at the shock transition.

In an accretion disc, transition of flow variables in the form of shock wave is manifested through the conservation laws of mass, momentum, energy and magnetic field (Sarkar & Das 2016, and reference therein). Across the shock front, these laws are explicitly expressed as the continuity of (a) mass flux ($\dot{M}_- = \dot{M}_+$), (b) the momentum flux ($W_- + \Sigma_- \upsilon_-^2 = W_+ + \Sigma_+ \upsilon_+^2$), (c) the energy flux ($\mathcal{E}_- = \mathcal{E}_+$) and (d) the magnetic flux ($\dot{\Phi}_- = \dot{\Phi}_+$), respectively, where the quantities with subscripts '$-$' and '$+$' refer their values before and after the shock. Here, we calculate the local energy of the flow as (Fukue 1990; Samadi et al. 2014)

$$\mathcal{E}(x) = \frac{\upsilon^2}{2} + \frac{a^2}{\gamma - 1} + \frac{\lambda^2}{2x^2} - \frac{1}{2(x-1)} + \frac{< B_\phi^2 >}{4\pi\rho}, \tag{20}$$

where all the quantities have their usual meaning. Employing these shock conditions, in the next figure, we calculate the shock location and its various properties knowing the flow parameters.

Towards this, we choose the flow parameters at the inner sonic point ($x_{\rm in}$) as in the case 'd' of Fig. 1. Following the method

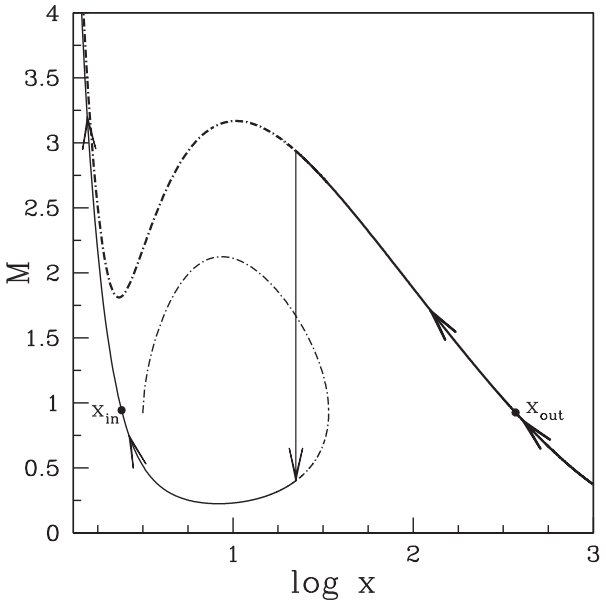

Figure 2. Illustration of a complete global accretion solution including shock transition in the $\log x - M$ plane. Inner sonic point ($x_{\rm in}$) and outer sonic point ($x_{\rm out}$) are marked. Arrows indicate the direction of the flow motion and the vertical arrow represents the shock transition. Flow parameters used here are same as Fig. 1(d). See the text for details.

described in Chakrabarti & Das (2004), using the shock conditions, we then uniquely determine the outer sonic point location ($x_{\rm out}$) and other flow variables of the accretion flow at $x_{\rm out}$ for the chosen inner sonic point. Utilizing these flow variables at $x_{\rm out}$, we integrate equations (13–16) outward up to the outer edge of the disc (chosen as $x = 1000$) in order to obtain a complete global accretion solution including shock waves. We present the result in Fig. 2, where Mach number (M) is plotted as a function of logarithmic radial distance. In reality, the obtained solution is needed to be visualized in the following way. The inflowing matter is injected subsonically from the outer edge of the disc at $x_{\rm edge} = 1000$. Flow becomes supersonic after crossing the outer sonic point at $x_{\rm out} = 369.98$ and continue to proceed towards the horizon. This is shown by the thick solid curve. Flow may continue its journey even further as shown by thick dotted curve, but eventually shock conditions are satisfied at $x_{\rm s} = 22.36$ and hence, supersonic flow undergoes discontinuous transitions in the form of shock waves to become subsonic. This is indicated by the vertical arrow. Due to gravity, subsonic flow again gains its radial velocity and ultimately enters in to the black hole supersonically after passing through the inner sonic point at $x_{\rm in} = 2.41$. This part of the solution is depicted using thin solid curve. In the figure, $x_{\rm in}$ and $x_{\rm out}$ are marked. Arrows indicate the overall direction of the flow motion towards the black hole. In the next figure, we examine the effects of the dissipation parameters ($\beta_{\rm edge}$ and/or $\dot{m}$) on the dynamics of shock location for flows with fixed initial parameters. In Fig. 3, inflowing matter is injected subsonically from the outer edge of the disc at $x_{\rm edge} = 500$ with specific energy $\mathcal{E}_{\rm edge} = 1.025 \times 10^{-3}$, angular momentum $\lambda_{\rm edge} = 0.1386\lambda_K$ and $\alpha_B = 0.02$. When the accretion rate and the plasma β at $x_{\rm edge} = 500$ are chosen as $\dot{m} = 0.0001$ and $\beta_{\rm edge} = 10^4$, respectively, flow encounter shock transition at $x_{\rm s} = 72.79$. In the figure, solid curve represents this result where the vertical arrow indicates the shock location. The corresponding inner and outer sonic points flow variables are given in Table 1. Next, we increase the accretion rate as $\dot{m} = 0.03$, keeping all the

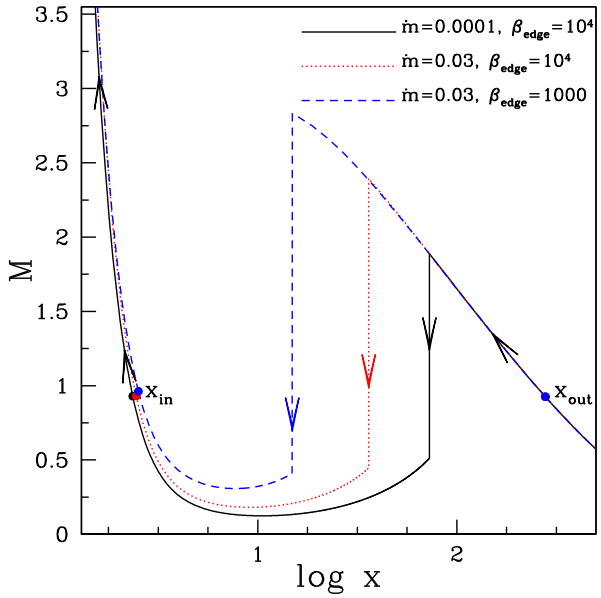

Figure 3. Variation of Mach number as function of logarithmic radial distance. Flows are injected from the outer edge $x_{\rm edge} = 500$ with energy $\mathcal{E}_{\rm edge} = 1.025 \times 10^{-3}$, angular momentum $\lambda_{\rm edge} = 0.1386\lambda_K$ and viscosity $\alpha_B = 0.02$. Solid, dotted and dashed curves depict the results obtained for $(\dot{m}, \beta_{\rm edge}) = (10^{-4}, 10^4)$, $(0.03, 10^4)$ and $(0.03, 10^3)$, respectively. Vertical arrows indicate the corresponding shock transitions positioned at $x_{\rm s} = 72.79$ (solid), $x_{\rm s} = 36.11$ (dotted) and $x_{\rm s} = 14.88$ (dashed). See the text for details.

Table 1. Flow variables measured at the sonic points for a shock induced global accretion solution. See the text for details.

Sonic point	x_c	λ_c	β_c	v_c	a_c
Inner	2.3550	$0.9392\lambda_K$	24.9315	0.153 33	0.164 95
Outer	278.3447	$0.1706\lambda_K$	6132.3040	0.026 48	0.028 598

Note. Subscript 'c' refers to the quantities measured at sonic points. For inner (outer) sonic point, 'c' is identified with 'in' ('out').

remaining flow parameters fixed at $x_{\rm edge}$ and observe that the shock front moves towards the horizon at $x_{\rm s} = 36.11$. This result is depicted using dotted curve where the dotted vertical arrow represents the shock transition. Increase of $\dot{m}$ evidently enhances the cooling rate of the flow. Since density and temperature of the flow are boosted up in the post-shock flow (PSC), effect of cooling at PSC is more intense compared to pre-shock flow and therefore, it reduces thermal pressure that causes the shock front to move close to the horizon in order to maintain pressure balance across the shock front. Further, we fix $\beta_{\rm edge} = 1000$ and $\dot{m} = 0.03$ keeping the other flow parameters unchanged at $x_{\rm edge}$ and obtain the shock location at $x_{\rm s} = 14.88$. We plot this result by the dashed curve, where the dashed vertical line denotes shock location as before. Lowering of $\beta_{\rm edge}$ demonstrates the increase of turbulent magnetic fields in the accretion flow that eventually leads to increase of Maxwell stress and therefore, the angular momentum transport from the inner part of the disc to the outer part of the disc is enhanced. This results the weakening of the centrifugal repulsion at PSC. Moreover, a decrease of $\beta_{\rm edge}$ eventually increases the synchrotron cooling efficiency as well. Overall, with the combined effects of both physical processes, shock front is pushed even further towards the horizon. This exhibits the fact that apart from $\dot{m}$, the role of $\beta_{\rm edge}$ is also important in determining the dynamics of shock location.

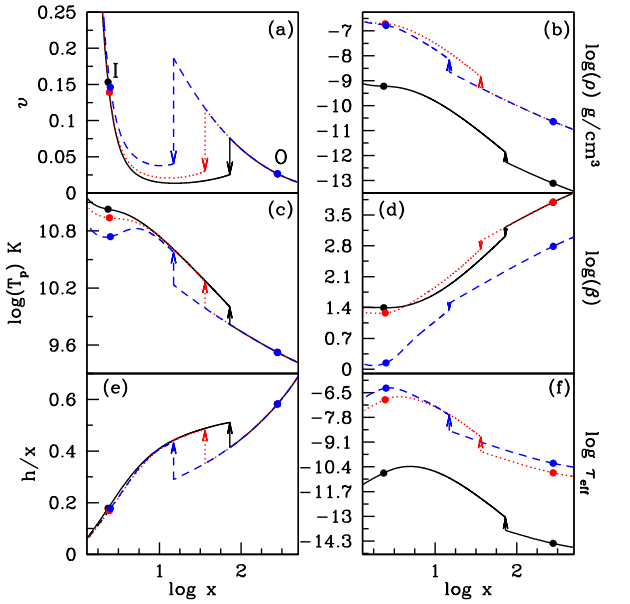

Figure 4. Variation of (a) radial velocity, (b) density in g/cm^3, (c) Temperature (d) ratio of gas pressure to magnetic pressure, (e) disc scaleheight (h/x) and (f) effective optical depth as function of logarithmic radial coordinate. Results plotted with solid, dotted and dashed curves correspond to the accretion solution depicted in Fig. 3. Filled circles represent the sonic points where the closer one is the inner sonic point and the furthest one is the outer sonic point. Vertical arrows indicate the shock position. See the text for details.

In Fig. 4, we illustrate the vertically averaged accretion disc structure corresponding to the solutions depicted in Fig. 3. In each panel, we plot the variation of a flow variable with logarithmic radial distance where the vertical arrows indicate the shock transition. Here, we consider $M_{\rm BH} = 10\,{\rm M}_\odot$ as a fiducial value. In Fig. 4(a), we demonstrate the radial velocity profile (υ) of the accretion flow. As expected, υ increases with the decrease of radial coordinate until it undergoes a shock transition. Across the shock, υ drops down to a subsonic value and again increases gradually in the post-shock region. Finally flow enters in to the black hole with velocity comparable to the speed of light after passing through the inner sonic point. Here, solid, dotted and dashed curves represent results for $(\dot{m}, \beta_{\rm edge}) = (10^{-4}, 10^4)$, $(0.03, 10^4)$ and $(0.03, 10^3)$, respectively. We show the density profile of the flow in Fig. 4(b), where we observe the rise of density immediately after the shock transition in all cases. This happens due to the reduction of radial velocity at PSC and eventually preserves the conservation of mass flux across the shock front. The overall density profile corresponding to $\dot{m} = 0.03$ is higher compared to the case of $\dot{m} = 10^{-4}$ simply because the large $\dot{m}$ stands for higher mass inflow at the outer edge. In Fig. 4(c), the proton temperature profile ($T_{\rm p}$) is shown. Across the shock front, supersonic pre-shock flow is turned into the subsonic flow and therefore, most of the kinetic energy of the infalling matter is converted to the thermal energy at PSC. This eventually leads to the heating of the PSC as indicated by the rise of post-shock temperature profile. Interestingly, when $\dot{m}$ is increased, the effect of cooling becomes more effective at PSC that causes the reduction of $T_{\rm p}$ as clearly seen close to the inner part of the disc. In addition, we observe that the decrease of $\beta_{\rm edge}$ essentially exhibits the reduction of the temperature profile of the accretion flow. This finding is in agreement with the results of numerical simulation (Machida et al. 2006), which yields a cooler disc structure for a magnetically dominated accretion flow.

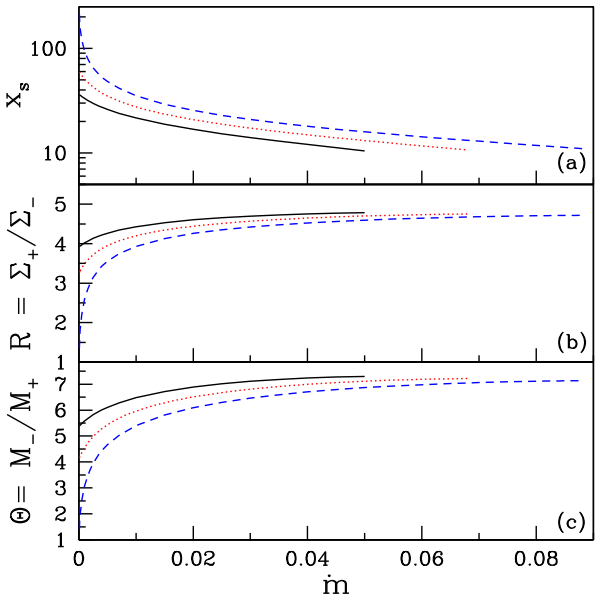

Figure 5. Variation of (a) shock location x_s, (b) compression ratio R and (c) shock strength Θ as function of $\dot{m}$ for flows injected from $x_{\rm edge} = 500$ with $\alpha_B = 0.02$, $\beta_{\rm edge} = 1400$ and $\mathcal{E}_{\rm edge} = 1.025 \times 10^{-3}$. Solid, dotted and dashed curves represent the results corresponding to $\lambda_{\rm edge} = 0.137\,57\lambda_K$, $0.138\,65\lambda_K$ and $0.139\,72\lambda_K$, respectively. See the text for details.

In Fig. 4(d), we show the radial variation of plasma β. We find that β decreases as the flow approaches to the black hole. Moreover, β falls down sharply across the shock that turns PSC into magnetically dominated. The radial dependence of the vertical scaleheight (h/x) is presented in Fig. 4(e). The validity of the thin disc approximation is observed all throughout from the outer edge to the horizon even in the presence of shock transition. Finally, in Fig. 4(f), we demonstrate the variation of effective optical depth, $\tau_{\rm eff} = \sqrt{\tau_{\rm es}\tau_{\rm syn}}$, where $\tau_{\rm es}$ represents the scattering optical depth given by $\tau_{\rm es} = \kappa_{\rm es}\rho h$ and the electron scattering opacity, $\kappa_{\rm es}$, is taken to be $\kappa_{\rm es} = 0.38\,{\rm cm^2 g^{-1}}$. Here, $\tau_{\rm syn}$ denotes the absorption effect arising due to thermal processes and is given by $\tau_{\rm syn} = \left(hq_{\rm syn}/4\sigma T_e^4\right)\left(2GM_{\rm BH}/c^2\right)$, where $q_{\rm syn}$ is the synchrotron emissivity (Shapiro & Teukolsky 1983) and σ is the Stefan–Boltzmann constant. We find that the optical depth of PSC is always greater than the pre-shock region as the density in the post-shock region is higher (see Fig. 4b). In addition, the overall variation of the optical depth for enhanced accretion rate remains higher all throughout. Moreover, in spite of the steep density profile, PSC is found to remain optically thin ($\tau < 1$). This apparently indicates that the possibility of escaping hard radiations from the PSC seems to be significant.

Fig. 5 illustrates the various shock properties as function of accretion rate ($\dot{m}$) for flows injected from a fixed outer edge as $x_{\rm edge} = 500$ with $\beta_{\rm edge} = 1400$, energy $\mathcal{E}_{\rm edge} = 1.025 \times 10^{-3}$ and viscosity $\alpha_B = 0.02$. In the upper panel (Fig. 5a), the variation of shock location is shown for three different values of angular momentum ($\lambda_{\rm edge}$) at $x_{\rm edge}$. The solid, dotted and dashed curves correspond to flows injected with angular momentum $\lambda_{\rm edge} = 0.137\,57\lambda_K$, $0.138\,65\lambda_K$ and $0.139\,72\lambda_K$, respectively. From the figure, it is evident that a wide range of $\dot{m}$ provides shock induced global accretion solutions. For a given $\lambda_{\rm edge}$, the shock position advances towards the horizon with the increase of accretion rate ($\dot{m}$). The increase of accretion rate enhances the efficiency of radiative cooling and the flow loses energy during accretion. Loss of energy leads to drop in post-shock thermal pressure and hence the shock front moves closer to the horizon in order to maintain pressure balance across the shock. When accretion rate has crossed its critical value ($\dot{m}^{\rm cri}$), standing shock fails to form as the shock conditions are no longer satisfied. This clearly provides an indication that the possibility of shock formation reduces with the increase of $\dot{m}$. It is to be noted that $\dot{m}^{\rm cri}$ does not possess a global value, instead it largely depends on the accretion flow parameters. Interestingly, when $\dot{m} > \dot{m}^{\rm cri}$, flow may contain oscillatory shocks, however, the analysis of non-steady shock properties are beyond the scope of this work. In addition, for a given $\dot{m}$, shock front moves outwards from the horizon when $\lambda_{\rm edge}$ is increased. This happens due to the fact that the centrifugal barrier becomes stronger with the increase of $\lambda_{\rm edge}$, which clearly indicates that the shocks are centrifugally driven.

It is already pointed out that the density and temperature of the PSC is increased due to the effect of shock compression. Moreover, the spectral properties of an accretion disc are directly dependent on the density and temperature distribution of the flow. Therefore, it is worthy to measure the amount of density and temperature enhancement across the shock transition. Towards this, we first compute the compression ratio, which is defined as the ratio of the vertically averaged post-shock density to the pre-shock density ($R = \Sigma_+/\Sigma_-$) and plot it as function of $\dot{m}$ in Fig. 5(b). The flow parameters are chosen as in Fig. 5(a). For fixed $\lambda_{\rm edge}$, R is found to increase monotonically with the increase of $\dot{m}$. This happens because shock front is pushed towards the horizon with the increase of $\dot{m}$ that boosted the density compression and subsequently increases the compression ratio. On the contrary, for fixed $\dot{m}$, when $\lambda_{\rm edge}$ is increased, shock recedes away due to the stronger centrifugal barrier causing the decrease of post-shock compression. Since shock ceases to exist for $\dot{m} > \dot{m}^{\rm cri}$, we observe a cut-off in R for all the cases. Next, we calculate the strength of the shock (Θ) which is defined as the ratio of pre-shock Mach number (M_-) to the post-shock Mach number (M_+) and it essentially measures the temperature jump across the shock. In Fig. 5(c), we show the variation of Θ as function of $\dot{m}$ for the same set of flow parameters as in Fig. 5(a). We find that the response of Θ on the increase of $\dot{m}$ is similar to R as described in Fig. 5(b).

In Fig. 6, we proceed to explore the shock properties in terms of $\beta_{\rm edge}$ for flows with same outer boundary values, namely, $x_{\rm edge} = 500$, $\mathcal{E}_{\rm edge} = 1.025 \times 10^{-3}$, $\alpha_B = 0.02$ and $\dot{m} = 0.01$. The solid, dotted and dashed curves represent results corresponding to $\lambda_{\rm edge} = 0.137\,57\lambda_K$, $0.138\,65\lambda_K$ and $0.139\,72\lambda_K$, respectively. Here also we observe that the shock front proceeds towards the horizon with the decrease of $\beta_{\rm edge}$ for all cases having different $\lambda_{\rm edge}$. When $\beta_{\rm edge}$ is reduced, the effect of synchrotron cooling is increased due to the increase of magnetic activity and therefore, shock moves inward. However, the indefinite reduction of $\beta_{\rm edge}$ is not possible keeping the remaining flow parameters unchanged because under a critical limit ($\beta_{\rm edge}^{\rm cri}$), shock ceases to exist. As in Fig. 5(b)–(c), here also we study the variation of compression ratio (R) and the shock strength (Θ) as function of $\beta_{\rm edge}$. We find that both R and Θ display anticorrelation relation with $\beta_{\rm edge}$.

Next, we study the properties of shock wave in terms of viscosity (α_B). While doing so, as before, we choose the flow injection parameter as $x_{\rm edge} = 500$, $\mathcal{E}_{\rm edge} = 1.025 \times 10^{-3}$, $\beta_{\rm edge} = 1400$ and $\dot{m} = 0.01$. We depict the results in Fig. 7 where solid, dotted and dashed curve are obtained for $\lambda_{\rm edge} = 0.137\,57\lambda_K$, $0.138\,65\lambda_K$ and $0.139\,72\lambda_K$, respectively. We observe that shock forms for a wide range of α_B. The shock position is reduced with the increase of α_B for all cases having different $\lambda_{\rm edge}$. Increase of α_B enhances the angular momentum transport outwards that causes the weakening of the centrifugal barrier and hence the shock is pushed towards

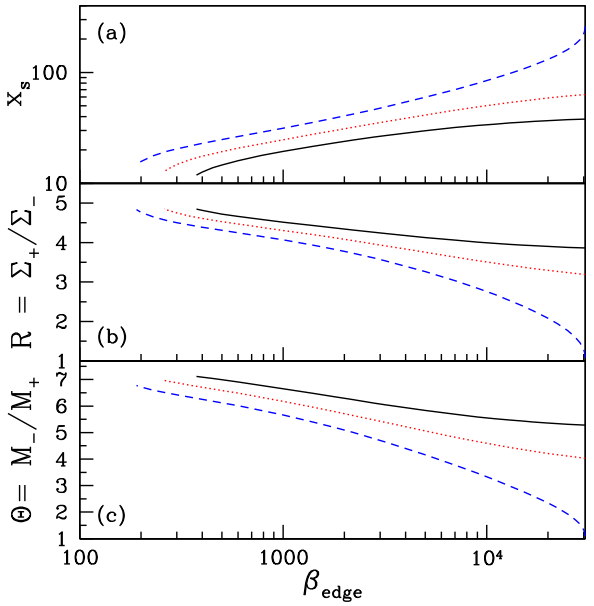

Figure 6. Variation of (a) the shock location x_s (b) shock compression ratio R and (c) shock strength Θ as function of β_{edge} for different values of λ_{edge}. Flows are injected from $x_{edge} = 500$ with $\mathcal{E}_{edge} = 1.025 \times 10^{-3}$, $\alpha_B = 0.02$ and $\dot{m} = 0.01$, respectively. Results depicted with solid, dotted and dashed curves are for $\lambda_{edge} = 0.137\,57\lambda_K$, $0.138\,65\lambda_K$ and $0.139\,72\lambda_K$, respectively. See the text for details.

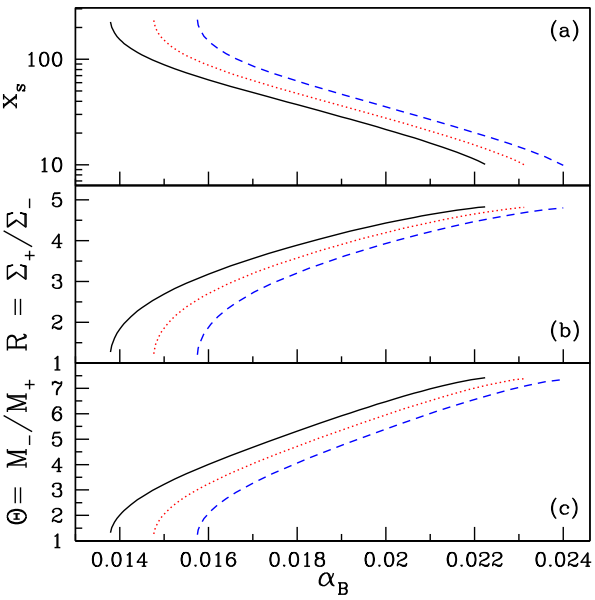

Figure 7. Variation of (a) the shock location x_s, (b) shock compression ratio R and (c) shock strength Θ as function of viscosity α_B for different values of λ_{edge}. Flows are injected from $x_{edge} = 500$ with $\mathcal{E}_{edge} = 1.025 \times 10^{-3}$, $\beta_{edge} = 1400$ and $\dot{m} = 0.01$. Results drawn with solid, dotted and dashed curves are for $\lambda_{edge} = 0.137\,57\lambda_K$, $0.138\,65\lambda_K$ and $0.139\,72\lambda_K$, respectively. See the text for details.

the horizon. When α_B is chosen beyond its critical value (α_B^{cri}), shock conditions are not satisfied and therefore, standing shock ceases to exist. Needless to mention that α_B^{cri} largely depends on the other accretion flow parameters. When $\alpha > \alpha_B^{cri}$, sub-Keplerian flow deviates from the Keplerian disc very close to the horizon and flow enters into the black hole after passing through a single sonic point. Further, we calculate the compression ratio (R) and the shock

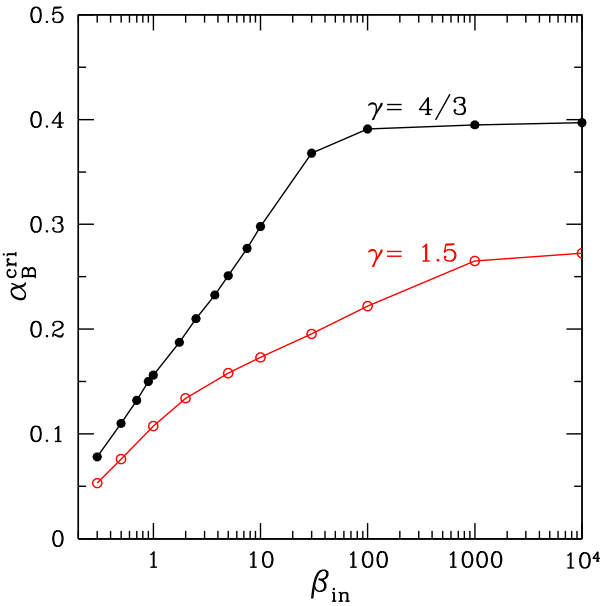

Figure 8. Variation of critical viscosity parameter (α_B^{cri}) as function of plasma β at inner sonic point (β_{in}) that allows standing shocks. Here, we choose $\dot{m} = 0.01$. Adiabatic indices are marked. See the text for details.

strength (Θ) for flows described in Fig. 7(a) and present the obtained results in Fig. 7(b)–(c). We observe that both R and Θ are gradually increased with α_B.

So far, we have examined the properties of shock induced global accretion solutions for flows having adiabatic index $\gamma = 4/3$. In reality, the limiting values of γ lie in the range between 4/3 and 5/3, depending on the ratio of the thermal energy and the rest energy of the flow (Frank, King & Raine 2002). Keeping this in mind, we now intend to compute the critical viscosity parameter (α_B^{cri}) as function of β_{in} that allows shocked accretion solution. While doing this, we consider thermally ultrarelativistic flow ($\gamma \sim 4/3$) and thermally seminon-relativistic flow ($\gamma \sim 1.5$) (Kumar & Chattopadhyay 2014; Yuan & Narayan 2014) and obtain α_B^{cri} for both the extreme cases as depicted in Fig. 8. Here, we assume $\dot{m} = 0.01$. Filled and open circles joined using the solid line represent the results corresponding to $\gamma = 4/3$ and 1.5, respectively. In a magnetized accretion flow with a given α_B, the transport of angular momentum towards the outer edge of the disc is increased with the decrease of β_{in} as the magnetic pressure contributes to the total pressure. Since shocks under consideration are centrifugally driven (see Fig. 5), therefore when β_{in} is small, a lower value of α_B is sufficient to transport the required angular momentum for shock formation. Evidently, α_B^{cri} possesses lower value for magnetized flow. As β_{in} is increased, α_B^{cri} is also increased and eventually approached towards a saturation value corresponding to the gas pressure dominated flow. For $\gamma = 4/3$, critical viscosity parameter tends to the asymptotic value $\alpha_B^{cri} \sim 0.4$ (Chakrabarti & Das 2004) and for $\gamma = 1.5$, the saturation value is found to be $\alpha_B^{cri} \sim 0.27$ (Das, Becker & Le 2009; Sarkar & Das 2016). We observe that α_B^{cri} is reduced as the flow changes its character from thermally ultrarelativistic ($\gamma = 4/3$) to thermally seminon-relativistic limit ($\gamma = 1.5$). This apparently indicates that the possibility of shock transition seems to be feeble when the flow approaches to the non-relativistic regime. This happens due to the fact that when γ tends to 5/3, flow possesses only single sonic point (Chakrabarti & Das 2004), thereby reducing the possibility of shock formation.

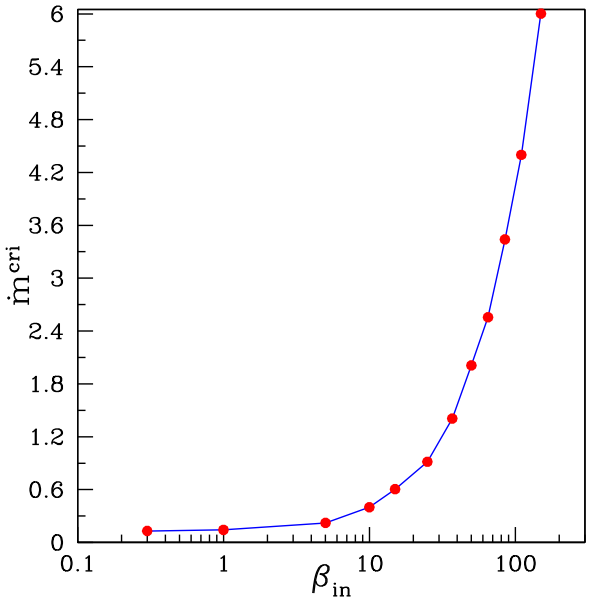

Figure 9. Variation of critical accretion rate $\dot{m}^{\rm cri}$ that allows standing shock as function of $\beta_{\rm in}$. Here, viscosity parameter is chosen as $\alpha_B = 0.01$. See the text for details.

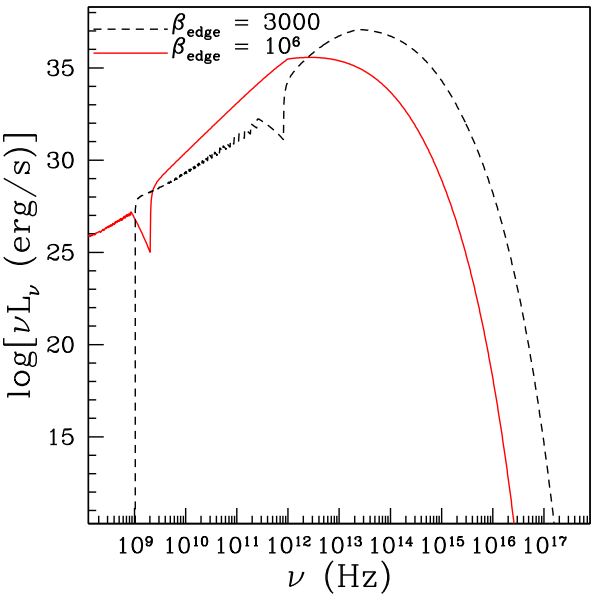

Figure 10. Typical spectra from an accretion disc around a black hole of mass $M = 10\,{\rm M}_\odot$ for a strong and weak accretion shock located at $x_{\rm s} = 13.14$ and 72.12, respectively. The two different shock locations correspond to flows injected from the outer edge with two different values of β as indicated in the figure. See the text for details.

We continue our investigation to calculate the critical accretion rate of the flow that provides the global accretion solutions including standing shock. In Fig. 9, we present the variation of critical accretion rate ($\dot{m}^{\rm cri}$) as function of plasma β measured at the inner sonic point ($\beta_{\rm in}$). Here, we choose viscosity parameter as $\alpha_B = 0.01$. In this analysis, we have chosen the wide range of β, where $\beta < 1$ represents the magnetic pressure dominated flow and $\beta > 1$ denotes the gas pressure dominated flow. Moreover, we consider synchrotron cooling as the effective radiative mechanism active in the flow. Since synchrotron process depends on both the strength of the magnetic fields and the density of accreting matter, one can obtain the required cooling effect by suitably tuning the density and the magnetic fields together. When $\beta_{\rm in} < 1$, the inner part of the disc becomes magnetically dominated as the disc is threaded with strong magnetic fields as compared to the gas dominated disc and therefore significant cooling effect can be achieved even with small accretion rate. Thus, for magnetically dominated flow, we obtain small values of $\dot{m}^{\rm cri}$. For example, we obtain the magnetic field at $x_{\rm in} = 2.5234$ as $B(x_{\rm in}) = 1.453 \times 10^7$ Gauss for $\lambda_{\rm in} = 0.978\,185\lambda_K$, $\alpha_B = 0.01$, $\beta_{\rm in} = 0.3$, $\dot{m}^{\rm cri} = 0.13$ and $M_{\rm BH} = 10\,{\rm M}_\odot$, respectively. As we gradually increase the value of $\beta_{\rm in}$, the effect of magnetic fields becomes weaker that eventually decreases the cooling effect in the flow. Hence, flow can sustain standing shock even with relatively large accretion rate. When $\beta \gg 1$, magnetic fields are very weak leading to the negligible cooling effect in the flow. Therefore, we are effectively left with a flow where $\dot{m}^{\rm cri}$ tends to become independent of $\beta_{\rm in}$ as observed in the figure.

In Fig. 10, we present the typical spectrum for shocked accretion flows injected from outer edge $x_{\rm edge} = 500$ with angular momentum $\lambda_{\rm edge} = 0.138\,65\lambda_K$ and energy $\mathcal{E}_{\rm edge} = 1.025 \times 10^{-3}$. Here, we consider viscosity as $\alpha_B = 0.02$ and accretion rate as $\dot{m} = 0.1$. For representation, black hole mass is chosen as $M_{\rm BH} = 10\,{\rm M}_\odot$. Considering $\beta_{\rm edge} = 10^6$, we obtain the global accretion solution where standing shock is formed at $x_{\rm s} = 72.12$. Following the works of Mandal & Chakrabarti (2005); Chakrabarti & Mandal (2006), we compute the disc synchrotron spectrum corresponding to this accretion solution and present it in Fig. 10 using solid curve. Further, we increase the effect of magnetic fields by setting $\beta_{\rm edge} = 3000$ and inject the flow keeping the remaining flow variables unaltered. We observe that the flow encounters standing shock transition at $x_{\rm s} = 13.14$. We then compute the disc spectrum as before and depict it in Fig. 10 using dashed curve. In both the cases, the pre-shock (low energy radiation) and post-shock (high energy radiation) synchrotron contributions are well separated across the sharp discontinuity due to sudden jump in temperature, density and magnetic field at the shock. The spikes in pre-shock contribution represent the cumulated cyclotron lines coming from different disc annuli. Evidently, lower β at outer boundary (dashed curve) corresponds to higher magnetic fields and therefore, the flow will be radiatively more efficient. Accordingly, the spectrum is shifted towards high energy for large magnetic field value. This essentially indicates that the disc is making a transition to a brighter hard state with the decrease of $\beta_{\rm edge}$. The above findings are in agreement with the results of Oda et al. (2012), where the brightening of the hard state is reported for disc that makes transition to the low-β state.

In the course of our investigation of accretion flow properties, we next put an effort to calculate the disc luminosity. Since we use the synchrotron emission as the potential cooling mechanism while modelling the accretion flows around black holes, the total surface disc luminosity ($L_{\rm disc}$) is estimated as

$$L_{\rm disc} = 4\pi \int_{x_i}^{x_{\rm f}} Q^- x {\rm d}x,$$

where the limit x_i refers to the location just outside the horizon and x_f stands for the outer edge of the disc, respectively, and Q^- denotes the synchrotron cooling rate. Here, for a given accretion rate ($\dot{m}$), we compute the maximum disc luminosity ($L_{\rm disc}^{\rm max}$) for shock and shock free accretion solutions by freely varying the remaining flow parameters and show its variation in units of Eddington luminosity as function of $\dot{m}$ in Fig. 11. Filled circles joined with the solid line represent the results corresponding to the global accretion solutions including shocks and the open circles connected with the dotted

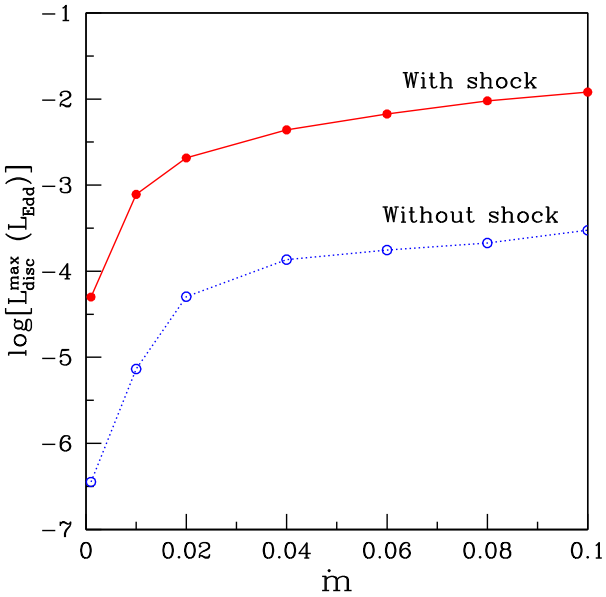

Figure 11. Variation of maximum disc luminosity $L_{\rm disc}^{\rm max}$ as a function of accretion rate $\dot{m}$. Filled circles connected with solid line denote the results for shocked accretion flows whereas the open circles joined with dotted line are for shock free accretion solutions. See the text for details.

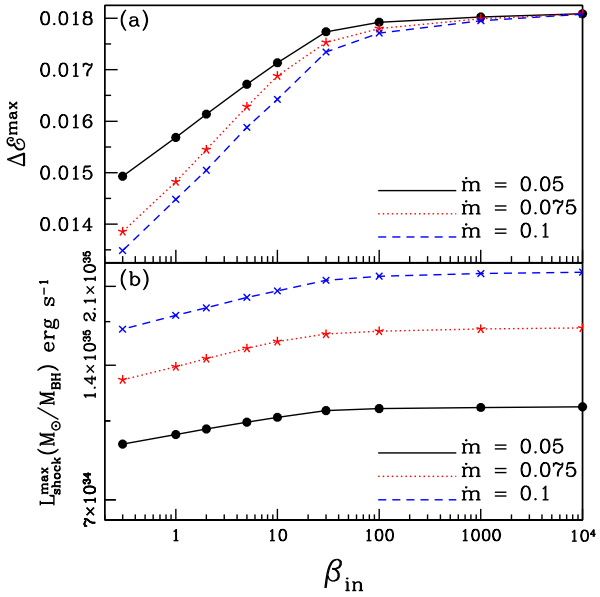

Figure 12. Variation of maximum energy dissipation at shock ($\Delta\mathcal{E}^{\rm max}$) as a function of β at inner sonic point ($\beta_{\rm in}$) for three different values of accretion rates, $\dot{m} = 0.05$, 0.075 and 0.1 denoted by solid, dotted and dashed curves, respectively.

curve are for shock free accretion solutions. Overall, we observe that $L_{\rm disc}^{\rm max}$ increases with $\dot{m}$ for all cases. This happens, simply because the increase of $\dot{m}$ manifests the rise of the flow density that eventually allows the flow to cool down more efficiently. Moreover, we find that for a fixed $\dot{m}$, $L_{\rm disc}^{\rm max}$ remains always higher for shocked accretion flows compared to the shock free flows. In other words, according to our model, the accretion flow containing shock waves are radiatively more efficient than the flows having no shock. Therefore, it is fairly indicative that the shocked accretion solutions seems to be potentially more preferred over the shock free solutions in explaining the energetics of black hole sources.

Until now, we have studied the various properties of accretion shock waves around black holes. These shocks are non-dissipative in nature as the specific energy remains conserved across the shock front (Chakrabarti 1989). Indeed, shocks of this kind are radiatively inefficient as well. Apparently, the realistic shock waves are likely to be dissipative, where a part of accreting energy is escaped from the shock location through the disc surfaces. This essentially causes the reduction of the overall specific energy profile in the PSC region (Singh & Chakrabarti 2011). The plausible mechanism that perhaps regulates the energy dissipation at the shock is the thermal Comptonization process (Chakrabarti & Titarchuk 1995) that eventually reduces the thermal energy in the PSC. Based on the above consideration, we assume that the loss of energy across the shock front is proportional to the temperature difference between the immediate pre-shock and post-shock flow and therefore, the energy loss across the shock front is calculated as (Das, Chakrabarti & Mondal 2010)

$$\Delta\mathcal{E} = fn\left(a_+^2 - a_-^2\right), \tag{21}$$

where a_- and a_+ denote the immediate pre-shock and post-shock sound speed and f represents the fraction of the available thermal energy lost at shock. In this analysis, we treat f as a free parameter and chose its value as $f = 0.998$ for representation. Evidently, this is the measure of energy dissipation across the shock (Das et al. 2010; Singh & Chakrabarti 2011; Sarkar & Das 2013; Kumar & Chattopadhyay 2013). We then compute the maximum energy dissipation ($\Delta\mathcal{E}^{\rm max}$) by freely varying all the flow parameters and plot it as function of $\beta_{\rm in}$ for various values of accretion rates in Fig. 12(a). Here, solid, dotted and dashed curves represent the results corresponding to $\dot{m} = 0.05$, 0.075 and 0.1, respectively. We observe that for a given accretion rate ($\dot{m}$), $\Delta\mathcal{E}^{\rm max}$ initially shows gradual increment with $\beta_{\rm in}$, which eventually approaches towards a saturation value in the gas pressure dominated domain. Meanwhile, it was shown by numerical simulation (Machida et al. 2006) that in the magnetically dominated state, accretion disc becomes cool as compared to a gas pressure dominated disc. This clearly indicates that the gas pressure dominated flow is expected to possess higher thermal energy content and accordingly, we obtain enhanced $\Delta\mathcal{E}^{\rm max}$ when $\beta_{\rm in}$ is larger. Moreover, as $\dot{m}$ is increased, cooling becomes more effective in the flow resulting the lowering of thermal energy content. Therefore, for a given $\beta_{\rm in}$, $\Delta\mathcal{E}^{\rm max}$ remains smaller for flows having higher $\dot{m}$. When $\beta_{\rm in}$ is large, the effect of synchrotron cooling due to the increase of accretion rate becomes practically insignificant. Hence, when $\beta_{\rm in} \to 10^4$, $\Delta\mathcal{E}^{\rm max}$ asymptotes to a saturation value irrespective to the flow accretion rate.

Next, we intend to infer the utility of dissipated energy at the shock ($\Delta\mathcal{E}$) in terms of the observable quantities. Indeed, a portion of the total usable energy available at the PSC is the same dissipative energy $\Delta\mathcal{E}$. Since jets are likely to be launched from the PSC, a part of this energy is used in the process of jet generation. Keeping this in mind, we calculate the maximum kinetic power lost by the disc corresponding to $\Delta\mathcal{E}^{\rm max}$ in terms of shock luminosity as $L_{\rm shock}^{\rm max} = \dot{M} \times \Delta\mathcal{E}^{\rm max} \times c^2$ erg s^{-1} (Le & Becker 2004, 2005; Sarkar & Das 2016). Here, $\dot{M}(\equiv \dot{m}\dot{M}_{\rm edd})$ represents the accretion rate in physical units. With this, in Fig. 12(b), we show the variation of the maximum shock luminosity (scaled with black hole mass) as a function of $\beta_{\rm in}$ for various accretion rates ($\dot{m}$). As before, solid, dotted and dashed curves represent the results corresponding to $\dot{m} = 0.05$, 0.075 and 0.1, respectively. Since we calculate the maximum shock luminosity using $\Delta\mathcal{E}^{\rm max}$, the obtained results apparently depend on the accretion rate although it manifests the variations similar to $\Delta\mathcal{E}^{\rm max}$ (see Fig. 12a). Consequently, we observe

that for a given $\beta_{\rm in}$, the maximum shock luminosity is increased with $\dot{m}$. Based on the above findings, we point out that our model calculation of shock luminosity (as depicted in Fig. 12b) can be readily used to understand the observational findings of core radio luminosity values associated with the black hole sources.

4 CONCLUSIONS

In this paper, we study the effect of synchrotron cooling in a magnetized advective accretion flow around a non-rotating black hole. While investigating the various properties of the accretion flow, since the origin of viscosity and the exact mode of angular momentum transport in accretion discs still remain inconclusive, we rely on the numerical simulation results of Machida et al. (2006) and assume that the $x\phi$-component of the Maxwell stress is proportional to the total pressure of the accreting matter. During accretion, flow changes its sonic state from subsonic to supersonic to become transonic before falling into the black hole. The position where flow becomes transonic is called as the sonic point. Depending on the input parameters, flow may pass through the multiple sonic points and the flow of this kind has the potential to exhibit shock phenomenon. Meanwhile, Oda et al. (2007, 2012) studied the global accretion solutions of magnetically supported accretion discs around stationary black holes. In these works, authors considered the accretion solutions that pass through the inner sonic point only. Essentially, these solutions are the subset of the generalized transonic accretion solutions as they ignored the flows containing multiple sonic points. Very recently, Sarkar & Das (2016) studied the properties of the shocked accretion flow considering bremsstrahlung cooling where magnetic field strength was assumed to be moderate throughout the flow. In this work, we calculate the shock induced global accretion solution for flows having wide range of plasma β parameters as $0.3 \leq \beta_{\rm in} \leq \infty$. With this, we further examine the effects of the dissipation parameters, namely viscosity (α_B) and accretion rate ($\dot{m}$), on the properties of global accretion solutions that contain shock waves. Such a study is important in the sense that the dissipation processes are likely to influence the spectral and timing properties of the radiation emitted from the disc (Chakrabarti & Manickam 2000; Nandi et al. 2001a,b, 2012; Radhika & Nandi 2014; Iyer, Nandi & Mandal 2015).

Our main concern here is to obtain the global magnetized accretion solution in presence of synchrotron cooling that contains shock wave (Fig. 2). For an accretion flow injected from a fixed outer edge, the dynamics of the shock front is regulated by cooling parameters, namely accretion rate ($\dot{m}$) and plasma β. Due to the presence of discontinuous shock transition, post-shock flow (i.e. PSC) is compressed resulting a hot and dense PSC. Therefore, when accretion rate and/or magnetic field are increased, cooling efficiency is enhanced causing the reduction of thermal pressure at PSC. This eventually compels the shock front to move towards smaller distance in order to balance the total pressure across the shock (Fig. 3). In our model solution, we find that the accretion flow is very hot, magnetized and optically as well as geometrically thin in the inner part of the disc (Fig. 4). This eventually allows the hard radiation to escape from PSC with ease. Moreover, we find that shock induced global accretion solutions are not the discrete solutions as shock forms for a wide range of flow parameters. Interestingly, above a critical limit of cooling parameters ($\dot{m}^{\rm cri}$ and $\beta^{\rm cri}_{\rm edge}$), PSC ceases to exist as the standing shock conditions fail to satisfy in presence of excess cooling (Figs 5–6).

Next, we put an effort to examine the properties of global shock solutions in both gas pressure as well as magnetic pressure dominated flow. While doing this, we calculate the critical viscosity parameter ($\alpha_B^{\rm cri}$) that caters standing shock waves. Here, we consider two different values of adiabatic index that represent accretion flow lying in the range between ultrarelativistic ($\gamma = 4/3$) to seminonrelativistic ($\gamma = 1.5$) domain. We observe that in all cases, $\alpha_B^{\rm cri}$ initially increases with $\beta_{\rm in}$ and asymptotically approaches to the saturation values $\sim$0.4 (for $\gamma = 4/3$) and $\sim$0.27 (for $\gamma = 1.5$), respectively for gas pressure dominated flow (Chakrabarti & Das 2004, King et al. 2007, Das et al. 2009, Kumar & Chattopadhyay 2013). Our steady model eventually establishes the fact that global shocks accretion solution can be obtained for fairly high viscosity parameter (Fig. 8).

We have further estimated the critical accretion rate ($\dot{m}^{\rm cri}$) that provides the global accretion solution including shock waves. We find that $\dot{m}^{\rm cri}$ is small for magnetically dominated flow as it is adequate to provide the required cooling efficiency that can sustain the standing shock in the accretion flow. As the strength of the magnetic field decreases, $\dot{m}^{\rm cri}$ gradually increases and ultimately $\dot{m}^{\rm cri}$ tends to become independent when magnetic fields are very weak leading to the gas pressure dominated flow (Fig. 9).

In Fig. 10, we have explored the typical spectrum of a magnetized accretion disc around black holes. For the purpose of representation, we consider two accretion flows having different magnetic field strengths. We find that the spectrum moves towards the high energy when magnetic field is large. This clearly indicates that the disc makes transition to the brighter hard state as the disc becomes magnetically dominated. In addition, we compare the disc luminosities for accretion solutions with and without shock and observe that shock accretion solutions are radiatively more efficient than the shock free solutions. This provides a possible hint that global shock solutions are potentially preferred over the shock free solutions in understanding the energetics of the black hole sources.

More important findings we examine in our steady state model when shocks under consideration are assumed to be dissipative in nature. In these circumstances, a part of the accreting energy is liberated at the shock which is allowed to escape through the disc surface. Interestingly, this available energy dissipated at shock can be used in powering the jets (Le & Becker 2004, 2005; Das et al. 2009). Following this, we self-consistently calculate the maximum radiative luminosity at shock ($L^{\rm max}_{\rm shock}$) corresponding to $\Delta\mathcal{E}^{\rm max}$ as an observable quantity and argue that the obtained results may be used to explain the observational findings of radio luminosities corresponding to the black hole sources.

At the end, we would like to point out that the present steady state formalism is developed based on several assumptions. For simplicity, we adopt pseudo-Newtonian potential to describe the space–time geometry around the black hole. We consider the adiabatic constant of the flow as global constant although it should be estimated self-consistently from the thermal properties of the accreting matter. In general, since the inner part of the disc is very hot and the radiative cooling time of relativistic electrons are shorter than the non-relativistic ions, the accreting plasma is expected to be characterized by two temperature flows. As the implementation of the above issues are beyond the scope of this paper, all these aspects will be the subject of our future study and will be reported elsewhere.

ACKNOWLEDGEMENTS

Authors thank the anonymous referee for useful comments and constructive suggestions.

REFERENCES

Akizuki C., Fukue J., 2006, PASJ, 58, 469
Aktar R., Das S., Nandi A., 2015, MNRAS, 453, 3414
Balbus S., Hawley J. F., 1991, ApJ, 376, 214
Balbus S. A., Hawley J. F., 1998, Rev. Mod. Phys., 70, 1
Becker P. A., Kazanas D., 2001, ApJ, 546, 429
Begelman M. C., Pringle J. E., 2007, MNRAS, 375, 1070
Bisnovatyi-Kogan G. S., Blinnikov S. I., 1976, Sov. Astron. Lett., 2, 191
Bisnovatyi-Kogan G. S., Ruzmaikin A. A., 1974, Ap&SS, 28, 45
Bu D. F., Yuan F., Xie F. G., 2009, MNRAS, 392, 325
Chakrabarti S. K., Titarchuk L., 1995, ApJ, 455, 623
Chakrabarti S. K., 1989, ApJ, 347, 365
Chakrabarti S. K., 1996, ApJ, 464, 664
Chakrabarti S. K., 1999, A&A, 351, 185
Chakrabarti S. K., Das S., 2004, MNRAS, 349, 649
Chakrabarti S. K., Mandal S., 2006, ApJ, 642, L49
Chakrabarti S. K., Manickam S. G., 2000, ApJ, 531, L41
Chattopadhyay I., Chakrabarti S. K., 2000, Int. J. Mod. Phys. D, 9, 717
Chattopadhyay I., Chakrabarti S. K., 2002, MNRAS, 333, 454
Chattopadhyay I., Chakrabarti S. K., 2011, Int. J. Mod. Phys. D, 20, 1597
Chattopadhyay I., Das S., 2007, New Astron., 12, 454
Das S., Chattopadhyay I., Nandi A., Molteni D., 2014a, MNRAS, 442, 251
Das S., 2007, MNRAS, 376, 1659
Das S., Chattopadhyay I., Chakrabarti S. K., 2001a, ApJ, 557, 983
Das S., Chattopadhyay I., Nandi A., Chakrabarti S. K., 2001b, A&A, 379, 683
Das S., Becker P. A., Le T., 2009, ApJ, 702, 649
Das S., Chakrabarti S. K., Mondal S., 2010, MNRAS, 401, 2053
Das S., Chattopadhyay I., Nandi A., Sarkar B., 2014b, Bull. Astron. Soc. India, 42, 39
Frank J., King A., Raine D. J., 2002, Accretion Power in Astrophysics. Cambridge Univ. Press, Cambridge
Fukue J., 1990, PASJ, 42, 793
Hirose S., Krolik J. H., Stone J. M., 2006, ApJ, 640, 901
Iyer N., Nandi A., Mandal S., 2015, ApJ, 807, 108
Johansen A., Levin Y., 2008, A&A, 490, 501
Khanna R., Camenzind M., 1996, A&A, 307, 665
King A. R., Pringle J. E., Livio N., 2007, MNRAS, 376, 1740
Krolik J. H., Hirose S., Blaes O., 2007, ApJ, 664, 1045
Kumar R., Chattopadhyay I., 2013, MNRAS, 430, 386
Kumar R., Chattopadhyay I., 2014, MNRAS, 443, 3444
Le T., Becker P. A., 2004, ApJ, 617, 25
Le T., Becker P. A., 2005, ApJ, 632, 476
Lynden-Bell D., 1969, Nature, 223, 690
Machida M., Nakamura K. E., Matsumoto R., 2006, PASJ, 58, 193
Mandal S., Chakrabarti S. K., 2005, A&A, 434, 839
Matsumoto R., Kato S., Fukue J., Okazaki A. T., 1984, PASJ, 36, 71
Miller J. M., Raymond J., Fabian A., Steeghs D., Homan J., Reynolds C., van der Klis M., Wijnands R., 2006, Nature, 441, 953
Mosallanezhad A., Abbassi S., Beiranvand N., 2014, MNRAS, 437, 3112
Nandi A., Chakrabarti S. K., Vadawale S. V., Rao A. R., 2001a, A&A, 380, 245
Nandi A., Manickam S. G., Rao A. R., Chakrabarti S. K., 2001b, MNRAS, 324, 267
Nandi A., Debnath D., Mandal S., Chakrabarti S. K., 2012, A&A, 542, A56
Narayan R., Kato S., Honma F., 1997, ApJ, 476, 49
Oda H., Machida M., Nakamura K. E., Matsumoto R., 2007, PASJ, 59, 457
Oda H., Machida M., Nakamura K. E., Matsumoto R., 2010, ApJ, 712, 639
Oda H., Machida M., Nakamura K. E., Matsumoto R., Narayan R., 2012, PASJ, 64, 15
Paczyński B., Wiita P. J., 1980, A&A, 88, 23
Radhika D., Nandi A., 2014, Adv. Space Res., 54, 1678
Sadowski A., 2016, MNRAS, 459, 4397
Samadi M., Abbassi S., Khajavi M., 2014, MNRAS, 437, 3124
Sarkar B., Das S., 2013, Astron. Soc. India Conf. Ser., 8, 143
Sarkar B., Das S., 2015, Astron. Soc. India Conf. Ser., 12, 91
Sarkar B., Das S., 2016, MNRAS, 461, 190
Shakura N. I., Sunyaev R. A., 1973, A&A, 24, 337
Shapiro S. L., Teukolsky S. A., 1983, Black Holes, White Dwarfs and Neutron Stars: The Physics of Compact Objects. Wiley, New York
Singh C. B., Chakrabarti S. K., 2011, MNRAS, 410, 2414
Torkelsson U., Brandenburg A., 1994, A&A, 283, 677
Yuan F., Narayan R., 2014, ARA&A, 52, 529

This paper has been typeset from a TEX/LATEX file prepared by the author.